Posted: September 5, 2020

Microstructure Analysis of Hybrid Laser Powder Bed Fusion and TIG Welding of Ni-based Superalloys

Ole Geisen[1], Jan Bogner[1], Ebrahim Ghavampour[1], María Teresa Pérez-Prado[2], Katharina Eissing[3], and Omar Fergani [*4]

[1]Siemens Gas and Power GmbH & Co. KG, Berlin, Germany
[2]IMDEA Materials Institute, Madrid, Spain
[3]Advanced Manufacturing Lab, ETH Zurich, Switzerland
[4]Siemens Digital Industries Software, Berlin, Germany

Abstract

The industrial use of laser powder-bed fusion (L-PBF) in turbomachinery is gaining momentum rendering the inspection and qualification of certain post-processing steps necessary. This includes fusion techniques that allow to print multiple parts separately to take advantage of e.g. various print orientations and join them subsequently. The main motivation of this study is to validate the tungsten inert gas (TIG) welding process of L-PBF manufactured parts using *industrial* specifications relevant for gas turbines to pave the way for the industrial production of modular build setups. For this, two commonly used nickel-based super alloys for high-temperature applications, Inconel 718 and Inconel 625 are chosen. Since their defect-free printability has been established widely, we focus on the suitability to be joined using TIG welding. The process is evaluated performing microstructural examination and mechanical tests in as-built as well as heat-treated samples. The welds are assessed by applying a general weld qualification approach used at Siemens Gas and Power. It was found that both materials can be joined via TIG welding using standard weld parameters causing minimal defects. A solution annealing heat treatment before welding is not necessary for a positive outcome, but still recommended for Inconel 718.

1 Introduction

L-PBF is an Additive Manufacturing (AM) technology which, due to the achievable feature resolution and processability of high-performance materials, is suited for gas turbine applications (1; 2). It is possible to produce L-PBF parts with similar mechanical and physical properties to those produced by conventional technologies such as casting (3). In addition, the technology allows for the manufacturing of highly complex and individualized components without the cost-intensive production of casting or forging molds for every design iteration (4). While the L-PBF technology comes with a lot of technical promises and opportunities, it still struggles to compete on an economical basis with already established production methods. Market studies have found that a drop in part production costs by a factor of ten is needed for the technology to become widely accepted in the industry (5). Aside from efforts to reduce production costs, it needs to be proven that the L-PBF technology can be integrated into a larger process chain for a widespread industrial adoption by various companies (6).

Many L-PBF applications for gas turbines today focus on the hot-gas path (9), where complex internal cooling features are employed, to utilize the design freedom of the technology (10). The use of L-PBF in rotating parts is still limited due to insufficient creep resistance of the materials available (11; 12; 13). While a common design approach in AM is to integrate multiple parts into one, subsequent joining is sometimes still required. The main reasons for using non-monolithic build-setups may be limitations of the build chamber size or avoiding support-structures, e.g. for internal structures, which may require specific build orientations for different features of a part. In both cases a modular build strategy can be beneficial. However, this creates the need for an adequate joining process in the subsequent assembly. In turbomachinery, as in all quality-conscious industries, both the material properties and the post-processing technologies, such as welding and joining, need to be qualified according to specifications.

[*]Corresponding author: o.fergani@gmail.com

Nickel superalloys Inconel 625 (IN625) and Inconel 718 (IN718) are commonly used in a wide variety of applications in turbomachinery and aerospace due to their relatively good corrosion resistance, excellent mechanical properties at elevated temperatures and weldability (16; 17). It has been well established that these materials can be manufactured by L-PBF without defects (28). In general, most L-PBF parts require a post-processing heat treatment to reduce residual stresses or to obtain the required structural performance, for example via recrystallization (IN625) or precipitation hardening (IN718). Although the chemical composition of IN625 and IN718 powders for L-PBF is the same as that corresponding to cast ingots, the different boundary conditions in the production process, such as the extreme cooling rates of the melt pools, give rise to different microstructures and properties (14). Analyses on relevant techniques such as TIG welding of conventionally manufactured parts out of these materials are well established and available (7). Additionally, the feasibility of laser welding of L-PBF manufactured parts was proven by Jokisch et al. (8). However, no studies on TIG-welding of L-PBF components using industrial specifications relevant for gas turbines have been published to date. Thus, investigating whether the metallurgical differences associated to L-PBF production methods have an influence on the quality of TIG-welds is timely.

The aim of this work is to investigate the applicability of TIG welding to Ni-superalloy components fabricated by L-PBF methods. Two scenarios of interest for gas turbine use cases are investigated and compared in this study, namely welding in the as-built condition or following a post-processing heat treatment. The first scenario has the potential to reduce the process chain complexity and is therefore interesting for industrialization. For both scenarios, the development of microstructure and the associated hardness were investigated on the cross-section areas of the weld seam.

2 Materials and Methods

Table 1: Chemical composition of Inconel 718 (18)

Chemical composition of IN718 in percent by weight						
Ni	**Cr**	**Nb**	**Mo**	**Ti**	**Al**	**Co**
50.0-55.0	17.0-21.0	4.75-5.5	2.8-3.3	0.65-1.15	0.2-0.8	≤ 1.0
Cu	**C**	**Si, Mn**	**P, S**	**B**	**Fe**	ρ $[g/cm^3]$
≤ 0.3	≤ 0.08	≤ 0.35	≤ 0.015	≤ 0.006	≤ 11.5	8.15

Table 2: Chemical composition of Inconel 625 (19)

Chemical composition of IN625 in percent by weight						
Ni	**Cr**	**Nb+Ta**	**Mo**	**O**	**Ti, Al**	**Co**
≥ 58.0	20.0-23.0	3.15-4.15	8.-10.0	≤ 0.03	≤ 0.4	≤ 1.0
Cu	**C**	**Si, Mn**	**P, S**	**N**	**Fe**	ρ $[g/cm^3]$
≤ 0.50	≤ 0.10	≤ 0.50	≤ 0.015	≤ 0.02	≤ 5.0	8.4

In this study, commercial IN718 powder from EOS GmbH (EOS Nickel Alloy IN718) and IN625 powder from LPW Technology Limited (LPW-625-AACP), both produced by gas atomization, were used. The chemical compositions are shown in Table 1 and Table 2, respectively. Both powder alloys contain fine-grained, spherical metal particles with properties suitable for L-PBF (15). The corresponding gaussian particle size distributions have a $d_{100} = 15 - 45 \mu m$.

Table 3: Chemical composition of Thermanit 625 (20)

Chemical composition of Thermanit 625 in percent by weight						
C	**Si**	**Cr**	**Mo**	**Ni**	**Nb**	**Fe**
≤ 0.02	≤ 0.02	22.0	9.0	Rest	3.5	1

L-PBF manufacturing was carried out in an EOS M290 machine, with a build envelope of 250x250x325 mm^3. The manufactured parts were pipes with a length of 100 mm, an outer diameter of 33.2 mm and a wall thickness of 1.6 mm. These dimensions were derived from Siemens specifications for weld qualification. All specimens were printed with EOS' standard parameters for IN718 at a layer thickness of $40 \mu m$ using argon as inert gas. The tubes were built vertically in multiple build jobs, as shown in Figure 1. Some L-PBF parts thus manufactured were additionally solid solution treated in order to investigate the effect of annealing on the weldability. A detailed list of the heat treatment conditions is specified for IN718 in Table 4 and for IN625 in Table 5.

As-built and heat treated samples were then TIG welded in the following way. A turning operation was first carried out to produce a V-seam weld preparation with an opening angle of 60°. TIG-welding of the pipes was then conducted manually in two layers in a PA (horizontal), PC (cross) and PH (vertically rising pipe) position (as per DIN EN ISO 6947) while a gap of approximately 2 mm was left between the specimens.

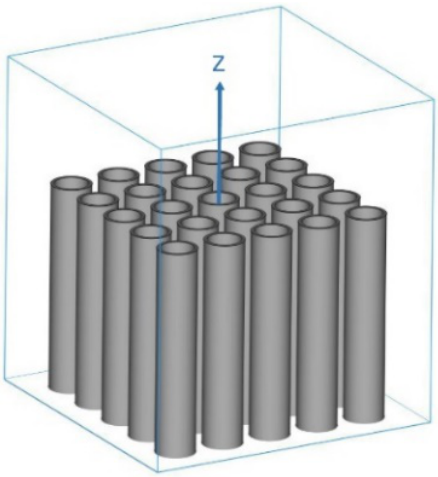

Figure 1: Welding procedure according to DIN EN ISO 9606-04 and welding positions according to DIN EN ISO 6947.

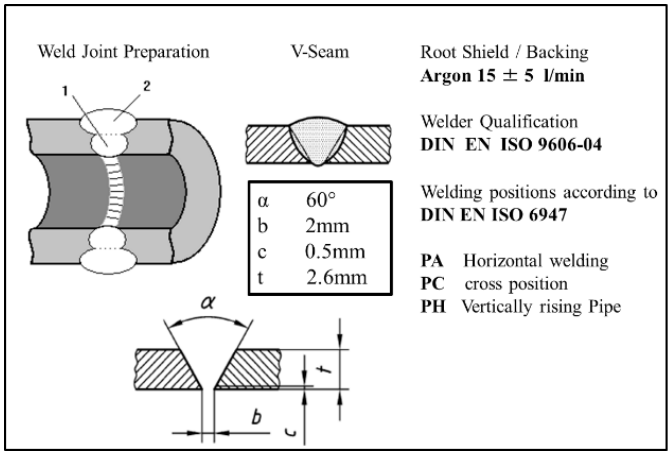

Figure 2: L-PBF build job setup of welding test specimens

The welding procedure including the welding positions is shown in Figure 2. Thermanit 625 (or UTP A 6222 Mo) was used as filler metal for all specimens. It is designed for weld joints of similar high-strength and corrosion-resistant nickel-based alloys. The chemical composition is listed in Table 3.

Table 4: Parameters for solution annealing heat treatment of IN718

	Program section	Process time [s]	Temperature [°C]	Heating/ cooling rate [°C/min]	Atmosphere
1	start	0	25		high vacuum
2	heating	6900	1175	10	high vacuum
3	storing	10500	1175		high vacuum
4	rapid cooling	11310	500	50	Argon
5	free cooling	20880	25		Argon

Table 5: Parameters for solution annealing heat treatment of IN625

	Program section	Process time [s]	Temperature [°C]	Heating/ cooling rate [°C/min]	Atmosphere
1	start	0	25		high vacuum
2	heating	4776	980	12	high vacuum
3	storing	8376	980		high vacuum
4	rapid cooling	8952	500	50	Argon
5	free cooling	17640	25		Argon

The weld joints were first inspected visually and by light microscopy. Figure 3 shows an image of the welded tubes obtained using a digital camera (Fig. 3a) as well as optical macrographs of two welds performed in as-built (Fig. 3b) and heat-treated (Fig. 3b) IN718. The cross sections were prepared with Kalling's 2 reagent to enhance the visibility of features under the bright field light microscopy. No major defects can be appreciated at this low magnification examination in any of the two materials investigated. The microstructure of the weld joints was also imaged by electron backscattered diffraction (EBSD) using a scanning electron microscope (SEM) equipped with an EBSD system, a CCD camera and the Channel 5.0 data acquisition and analysis software package. The presence of microstructural gradients in welds may lead to local variations of the hardness, which might reach levels that are detrimental for a component's life. According to the DIN EN ISO 15614-1 norm the maximum permissible values for Ni-based alloys are 450 HV for non-heat-treated samples and 350 HV for heat-treated parts (21). However, according to internal specifications, an HV value above 375 is not permissible for the purpose of this test. In this study, the Vickers hardness (22) was measured on a cross section of the welds according to DIN EN ISO 9015-1 (23). Instead of the ten indentations required by the norm, 21 measurements were performed for a more detailed analysis. The measurements were carried out using a test load of 1 kgf (HV) and a holding time of 10 s (24).

3 Results and discussion

Figure 4 illustrates an Inconel 718 cut weld seam in the as-built condition. The structural differences between the base material (BM), the heat-affected zone (HAZ) and the weld zone (WZ) can be noted visually. As shown in 4b, melt pools can be clearly distinguished in the BM of the L-PBF manufactured pipes. Some pores can be seen close to the surface in the BM. However, melt pool boundaries are no longer visible in

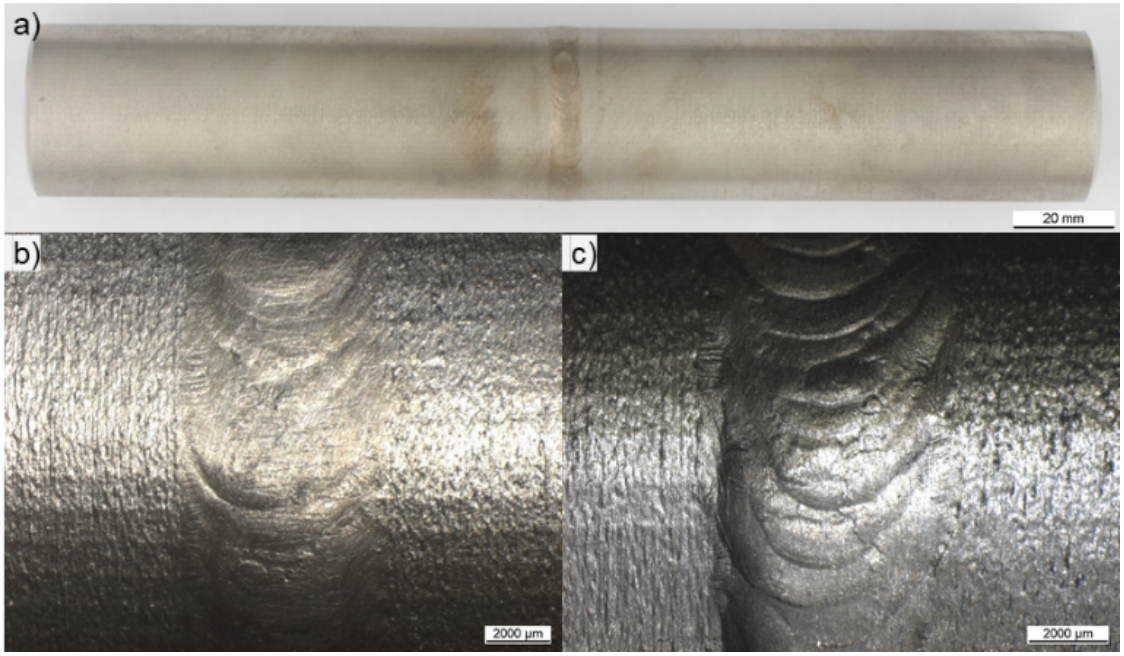

Figure 3: Two pipes TIG-welded together (a), Light microscopy photo (10x) of a weld seam of non-heat treated (b) and heat-treated IN718 (c).

the HAZ, revealing the occurrence of microstructural changes as a consequence of welding (Fig.3c). Pores can also be found in the HAZ, close to the weld seam. The IN625 welds in the as-built condition exhibit a similar appearance at this magnification.

Figures 5 and 6 show the microstructure of the IN718 and IN625 welds, respectively, in the as-built condition. In both cases, EBSD inverse pole figure maps in three perpendicular directions are given. The horizontal direction in the map (X) is parallel to the building direction. The corresponding inverse pole figures are also included in these figures. The latter were determined for the entire area of the EBSD maps and accordingly indicate the crystallographic preferential orientations for all zones (BM, HAZ, WZ). It must be noted here that, since the grains in the WZ, especially those in the root layer, occupy a relatively large volume, they have a large influence on the inverse pole figure. In both materials, the BM and HAZ are populated with grains that are elongated along the building direction, and possess a typical crystallographic texture, in which the building direction is mostly parallel to a <001> direction, as is usually observed in L-PBF manufactured Ni superalloys (28; 29). Overall, the grain size within the WZ is significantly larger than that of the BM and HAZ. The WZ is formed by two layers. The root layer consists mostly of equiaxed grains, while the grains at the top layer are elongated along the direction of thermal flow. Within the WZ, in the IN718 weld, the large grains at the root layer have a tendency to orient with a [001] direction parallel to all three perpendicular axes examined. In the IN625 alloy the grains at the root layer are, however, more randomly oriented and slightly smaller in size.

Figure 7 depicts an IN718 cut weld seam in the heat-treated condition. At least visually, the difference between the BM (Fig.7b) and the HAZ (Fig.7c)) is much less pronounced for the heat-treated compared to the non-heat-treated pipes. The heat treatment of the BM caused a visible change in the components' texture. As shown in Fig. 7b, the scale-like surface-structure is no longer visible. Instead, a more homogenous structure can be seen. Some pores can still be found in the BM, in regions located near the surface. The IN625 welds in the heat treated condition exhibit a similar appearance at this magnification.

Figures 8 and 9 illustrate the microstructure of the IN718 and IN625 welds, respectively, in the heat treated condition. In both cases, again, EBSD inverse pole figure maps in three perpendicular directions, as well as the corresponding inverse pole figures, are given. Here, also, the building direction is parallel to the horizontal direction. The inverse pole figures were also determined for the entire area of the EBSD maps and, accordingly, indicate the crystallographic preferential orientations for all zones (BM, HAZ, WZ). The heat treatment is observed to have a clear effect in the microstructure of the BM and the HAZ, whose textures become clearly weaker, especially in the case of the IN625 material, where, simultaneously, elongated grains are replaced by more equiaxed and irregularly shaped crystallites. The grain size within the

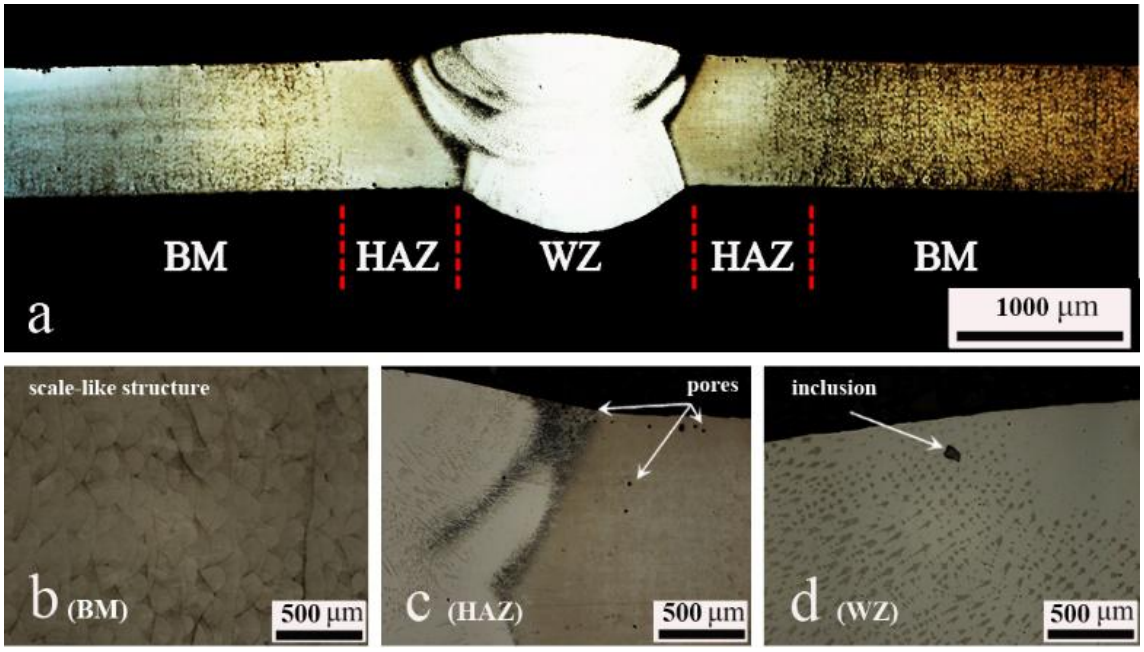

Figure 4: Light microscope images of cross sections of the IN718 specimen without heat treatment a) Overview b) Base material with typical flake structure c) Heat-affected zone with pores d) Weld seam with inclusion.

WZ remains significantly larger than that of the HAZ and BM. Within the WZ the main difference observed is the partial replacement of the elongated grains at the uppermost layer of the IN718 weld by smaller and more equiaxed crystallites, endowed with random orientations. The mentioned elongated shape is, however, retained in the IN625 WZ. In summary, our data reveal that the heat treatment seems to affect significantly the microstructure and the texture of the BM and HAZ zones and that its effect on the WZ is less noticeable.

The observed weakening of the texture of the BM and HAZ zones, which is more pronounced in the IN625 alloy, may be attributed to the occurrence of discontinuous recrystallization. This process consists on the long-range migration of high angle boundaries, thus facilitating the nucleation and growth of strain free grains with orientations that are different from those present in the as-built material (30). Partial discontinuous recrystallization is likely also the micromechanism that leads to the appearance of randomly oriented grains at the uppermost layer of the IN718 weld. The feasibility of recrystallization during post-processing heat treatments in SLM processed materials is highly dependent on the amount of strain energy stored during fabrication, which varies with process parameters and material types. Earlier works have demonstrated the occurrence of recrystallization in IN718 and IN625 samples fabricated by L-PBF processes following a solution treatment at similar temperature and holding time as those utilized in the present study e.g. (31; 32; 33). Amato et al.(31),in particular, reported a degree of recrystallization of about 50 percent. Luo et al. (32) confirm the presence of recrystallized grains when the solution treatment temperature exceeds 940 °C. Furthermore, they report that when the solution annealing temperature is increased to 980 °C, a large number of recrystallized grains appear at the boundaries of laser scanning tracks and, consequently, the latter become faintly visible. This is consistent with the absence of melt pool traces in the BM and HAZ of the heat treated samples of the present study (Fig. 7), in which the solution temperatures were 1175 °C for IN718 and 980 °C for IN625. Additionally, Li et al. (33) report that recrystallized grains in L-PBF processed and solution treated IN625 have random orientations. The microstructural evolution of the BM and HAZ of the Ni superalloys investigated here are fully consistent with earlier works.

The absence of significant microstructural evolution upon heat treatment within the WZ of the investigated materials is consistent with the presence in these zones of lower levels of stored energy as a consequence of grain growth during welding, resulting in a smaller driving force for recrystallization. The observed lack of significant microstructural change reveals, instead, that only recovery processes, which are not detectable in the EBSD maps provided here as they involved only dislocation rearrangement processes.

The local variation of the Vickers hardness was evaluated in the Ni-superalloy welds, both in the as-built

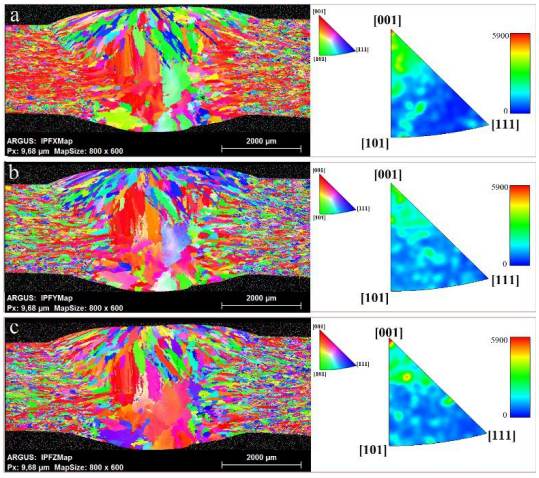

Figure 5: EBSD measurements of cross section of IN718 specimen without solution annealing heat treatment;
a) IPFX map with inverse pole figure of X direction
b) IPFY map with inverse pole figure of Y direction
c) IPFZ Map with inverse pole figure of Z direction.

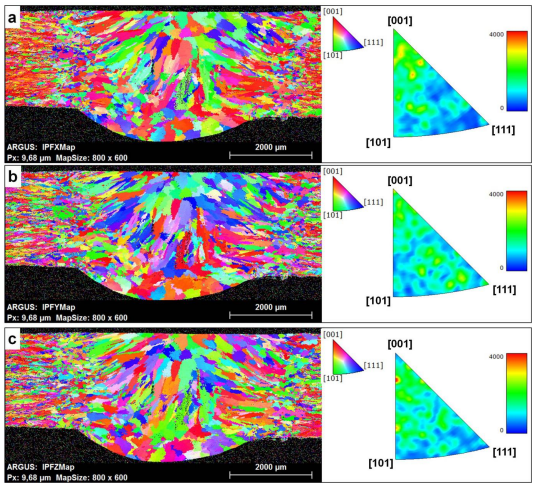

Figure 6: EBSD measurements of cross section of IN625 specimen without solution annealing heat treatment;
a) IPFX map with inverse pole figure of X direction
b) IPFY map with inverse pole figure of Y direction
c) IPFZ Map with inverse pole figure of Z direction.

and heat treated conditions. The cross area of the welds was segmented for hardness evaluation as indicated in the upper part of Fig. 10. The corresponding HV-values are given also in the same figure. Several observations can be made here. First, as expected, in the as-built condition the hardness is lower in the WZ than in the HAZ and BM due to the presence of significantly larger grains. Indeed, the U-shape of the hardness curves corresponding to the as-built materials indicates a negative correlation between grain size and measured hardness, in agreement with the well-known Hall-Petch relationship. The difference between the three measurement planes (D1, D2, D3) is only marginal. Following solution annealing, however, the hardness values decrease noticeably in the BM and HAZ regions in both materials, while they remain relatively constant in the WZ. In particular, in IN718 the hardness decreases in the BM by approximately 70 HV while in the same region of IN625 it decreases by approximately 100 HV. The hardness of all WZ areas ranges between 210 and 240 HV. These differences can be explained by the variability of the manual welding process. Investigations by Ramkumar et al. concerning the weldability of conventionally manufactured IN625 sheets with AISI 304 sheets using the TIG method, with the same filler material used in this study, measured hardness values around 210 and 250 HV in the WZ (27). Thus, there appears to be no significant difference in the measured hardness of the weld metal when comparing conventionally and L-PBF manufactured parts.

The observed changes in the hardness values following annealing are fully consistent with the microstructural evolution reported above. Discontinuous recrystallization is usually accompanied by a significant decrease in the hardness, as strain hardened grains are replaced by growing strain free crystallites. Recovery processes, instead, lead only to minor changes in the materials properties (30). Thus, the significant decrease in the hardness observed in the BM and HAZ areas can be rationalized by the occurrence of recrystallization in those regions. On the other hand, the negligible change in the hardness of the WZ that follows the solution treatment may be attributed to the occurrence of recovery processes and to the absence of recrystallization.

In summary, this study demonstrates the weldability of both Ni superalloys using the TIG method. A weld parameter variation outside of the standard parameters is thus not needed. Both, IN718 and IN625, can be TIG-welded using the same welding parameters and materials. Visually no major defects could be seen on any weld seam, regardless of the material and heat treatment. Although no local hardness peaks were found in any of the specimens, the as-built IN718 exhibits hardness values close to the permissible limit of 375 HV in the BM. Hence, a heat treatment before or after welding is not necessary, but still recommended. This is consistent with the fact, that the IN718 is used in its γ'' hardened form in most cases, meaning that the production setup without any heat treatment has no relevance in the industry today. The near-surface porosity in all specimens is thought to be caused by a suboptimal contour scanning strategy, which has been addressed in new parameter developments thereafter.

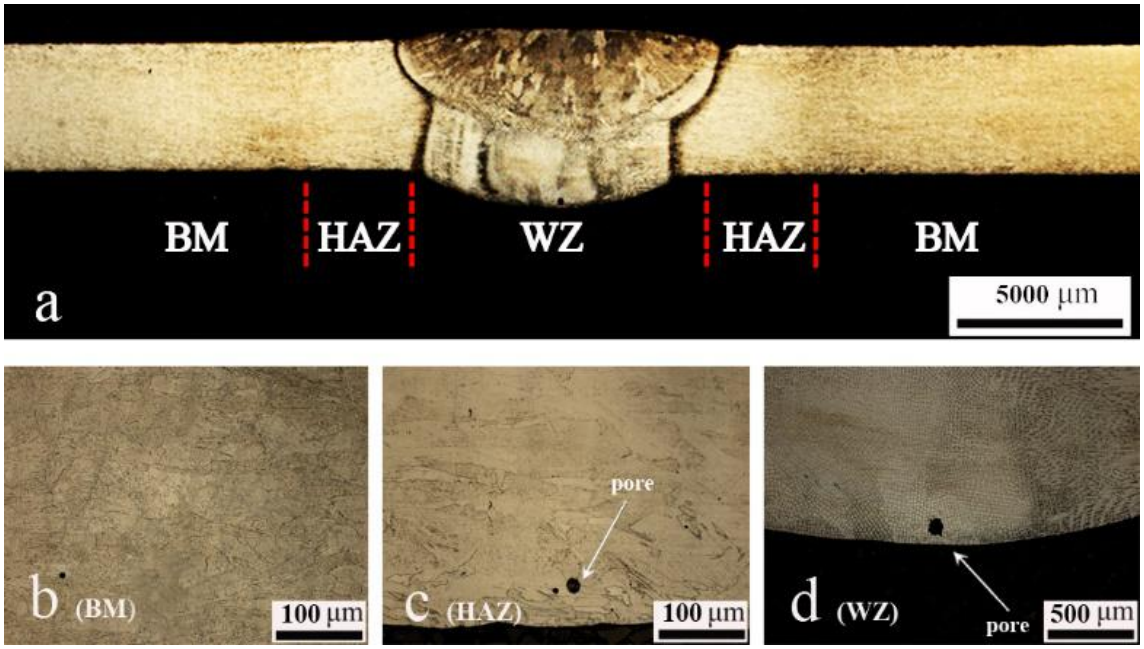

Figure 7: Light microscopic images of the cross sections etched with Kalling's 2 in brightfield for IN718 with heat treatment a) Overview; b) Base material c) Heat-affected zone with pore d) Weld seam with pore

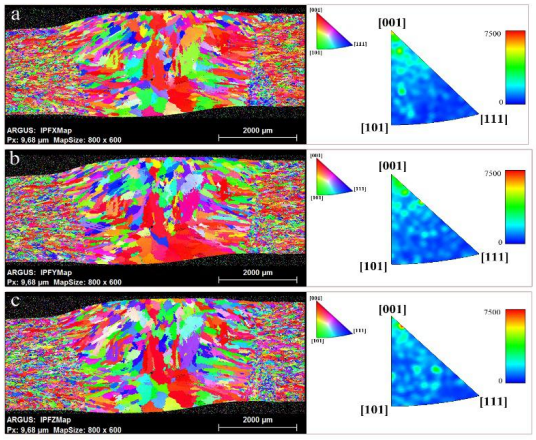

Figure 8: EBSD measurements on cross section IN718 with solution annealing heat treatment;
a) IPFX Map with inverse pole figure of X direction;
b) IPFY Map with inverse pole figure of Y direction;
c) IPFZ Map with inverse pole figure of Z direction.

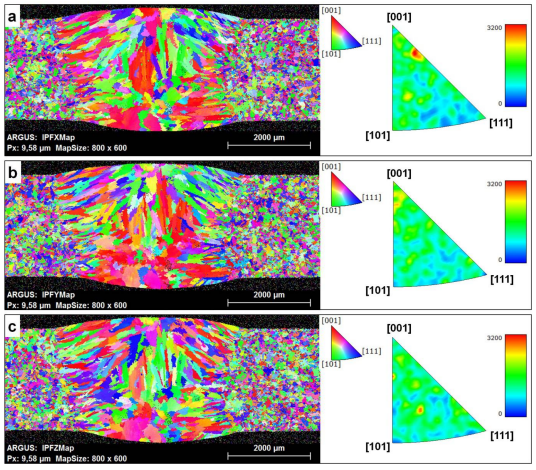

Figure 9: EBSD measurements on cross section IN625 with solution annealing heat treatment;
a) IPFX Map with inverse pole figure of X direction;
b) IPFY Map with inverse pole figure of Y direction;
c) IPFZ Map with inverse pole figure of Z direction.

4 Conclusions

The weldability of L-PBF manufactured pipes made of IN718 and IN625 using TIG welding has been demonstrated in this study. No defects or weak points, which would preclude a process qualification according to industry standards, have been discovered. Both materials are applicable for production by laser powder-bed fusion and subsequent tungsten inert gas welding. The results show that heat treatment is not necessary for a positive welding result. However, heat treatment is recommended for IN718. Based on the results of this study, a full qualification of a process chain involving TIG welding of L-PBF manufactured parts into bigger assemblies is to be expected. This study is an early step toward integrating the L-PBF technology into mass production chain process. Further research is required in order to fully industrialize the technology. For future studies, we recommend investigations on the mechanical properties of TIG-welded tensile test bars produced by L-PBF. Additionally, welding tests combining L-PBF with wrought or cast materials can be

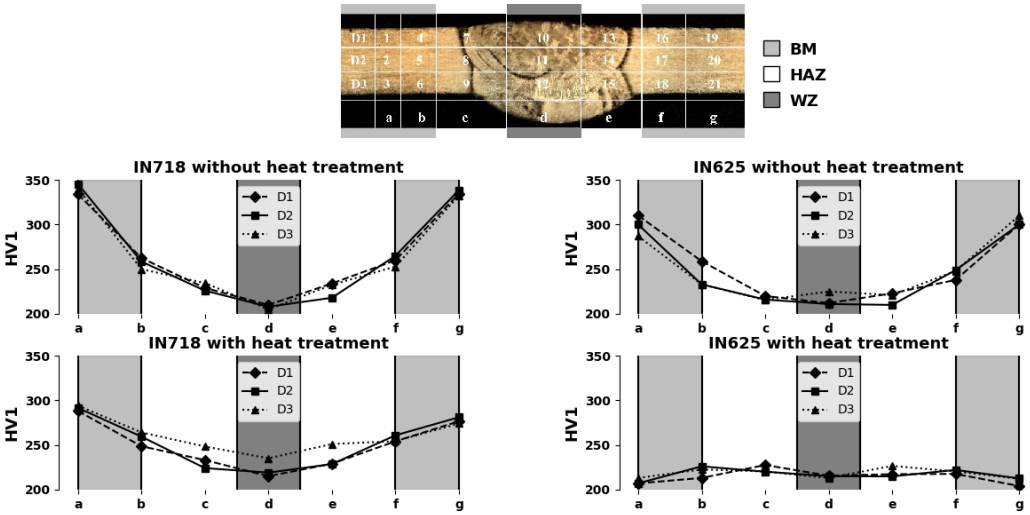

Figure 10: Top: Hardness measurement locations, Bottom: Vickers Hardness at the cross sections of IN625 and IN718 with and without heat treatment.

interesting for certain use cases and should be carried out as described in this study.

Acknowledgment

We would like to thank Carsten Geisler for the contributions during his time with Siemens.

Abbreviations

The following abbreviations are used in this manuscript:

AM	Additive Manufacturing
L-PBF	Laser Powder-Bed Fusion
IN718	Inconel 718
IN625	Inconel 625
TIG	Tungsten Inert Gas
HAZ	Heat Affected Zone
BM	Base Material
WZ	Weld Zone
EBSD	Electron Backscatter Diffraction
IPF	Inverse Pole Figure
HV	Vickers Hardness
NDT	Non-Destructive Testing

References

[1] Brandt, Milan. Laser additive manufacturing: Materials, Design, Technologies and Applications. Elsevier, Woodhead, Amsterdam (2017).

[2] D. Day, E. Kawecki, J.R. McNally, T.J. Rosenbarger, Day, David, Kawecki, Edwin, McNally, Joshua R., and Rosenbarger, Thomas J. “Development and Material Characterization of an Additively Manufactured Nickel Alloy for Turbine Applications.” (2018). DOI 10.1115/GT2018-76614.

[3] J.-P. Kruth, M. Badrossamay, E.Yasa, J. Deckers, L. Thijs, J. Van Humbeeck. “Part and material properties in selective laser melting of metals.”, 16th International Symposium on Electromachining (ISEM XVI), Shanghai, China (2010).

[4] J. Geraedts, Z. Doubrovski, J.C. Verlinde, M.C. Stellingwerff. “Three views on additive manufacturing: Business, Research and Education.” (2012).

[5] B. Langefeld, M. Moehrle, C. Balzer, P. Schildbach. “Advancements in metal 3D printing: Beyond powder bed – Additive manufacturing on the brink of industrialization.” (2018).

[6] Niaki, Mojtaba Khorram, Torabi, S. Ali, and Nonino, Fabio. “Why manufacturers adopt additive manufacturing technologies: The role of sustainability.” Journal of Cleaner Production Vol. 222 (2019): pp. 381–392. DOI 10.1016/j.jclepro.2019.03.019.

[7] Ogborn, J. S., Olson, D. L., and Cieslak, M. J. “Influence of solidification on the microstructural evolution of nickel base weld metal.” Materials Science and Engineering: A Vol. 203 1-2 (1995): pp. 134–139. DOI 10.1016/0921-5093(95)09832-1.

[8] Jokisch, Torsten, Marko, Angelina, Gook, Sergej, Üstündag, Ömer, Gumenyuk, Andrey, and Rethmeier, Michael. “Laser Welding of SLM-Manufactured Tubes Made of IN625 and IN718.” Materials (Basel, Switzerland) Vol. 12 No. 18 (2019). DOI 10.3390/ma12182967.

[9] J. Schurb, T. Etter, K.K. Urban, M. Höbel. “Additive Manufacturing for Hot Gas Path Parts.” (2016, Brussels).

[10] W. Fu, C. Haberland, E.V. Klapdor, D. Rule, S. Piegert. “Streamlined Frameworks for Advancing Metal Based Additive Manufacturing Technologies in Gas Turbine Industry.” (2017 Zurich).

[11] K. Kunze, T. Etter, J Grässlin, V. Shklover. “Texture, anisotropy in microstructure and mechanical properties of IN738LC alloy processed by selective laser melting (SLM).” Materials Science and Engineering: A Vol. 620 (2014): pp. 213–222. DOI 10.1016/j.msea.2014.10.003.

[12] Luke Nelson Carter. “Selective laser melting of nickel superalloys for high temperature applications.”.

[13] Y. Kuo, T. Nagahari, K.Kakehi. “The Effect of Post-Processes on the Microstructure and Creep Properties of Alloy718 Built Up by Selective Laser Melting.” Materials (Basel, Switzerland) Vol. 11 No. 6 (2018). DOI 10.3390/ma11060996.

[14] Risse, Jeroen. “Additive Fertigung der Nickelbasis-Superlegierung IN738LC mittels selektivem Laserstrahlschmelzen.”. RWTH Aachen University. DOI 10.18154/RWTH-2019-06822.

[15] Schatt, Werner, Wieters, Klaus-Peter, and Kieback, Bernd. Pulvermetallurgie: Technologien und Werkstoffe. Springer, Berlin (2007).

[16] M. Liu, W. Zheng, J. Xiang, Z. Song, E. Pu, H. Feng. “Grain Growth Behavior of Inconel 625 Superalloy.” Journal of Iron and Steel Research International Vol. 23 No. 10 (2016): pp. 1111–1118. DOI 10.1016/S1006-706X(16)30164-9.

[17] X. Zhao, J. Chen, X. Lin, W. Huang. “Study on microstructure and mechanical properties of laser rapid forming Inconel 718.” Materials Science and Engineering: A Vol. 478 1-2 (2008): pp. 119–124. DOI 10.1016/j.msea.2007.05.079.

[18] Electro Optical Systems GmbH. “Materialdatenblatt: EOS NickelAlloy IN718.” (2011).

[19] LPW technolgy. “LPW Powders Brochure: AM metal powders from LPW.” (2017).

[20] EN ISO 18274. “Eigenschaften und Anwendungsgebiete UTP A 6222.”.

[21] Anforderung und Qualifizierung von Schweißverfahren für metallische Werkstoffe - Schweißverfahrensprüfung.

[22] Schubert, Reinert, Egberts, Dyck. “Unterlagen für den Laborversuch der Härteprüfung: Hochschule Bremen University Of Applied Sciences.”.

[23] CENELEC Management Centre. “DIN EN ISO 9015-1: Zerstörende Prüfung von Schweißverbindungen an metallischen Werkstoffen. Teil 1: Härteprüfung für Lichtbogenschweißverbindungen (ISO 9015-1:2001).” (2011).

[24] CENELEC Management Centre. “DIN EN ISO 6507-1: Metallic materials - Vickers hardness test. Part 1: Test method (ISO 65071:2018).” (2005 Oktober).

[25] C.E. Seow, H.E. Coules, G. Wu, R.H.U. Khan, X. Xu, S. Williams. “Wire + Arc Additively Manufactured Inconel 718: Effect of post-deposition heat treatments on microstructure and tensile properties.” Materials & Design Vol. 183 (2019): pp. 108–157. DOI 10.1016/j.matdes.2019.108157.

[26] D.E. Cooper. “The High Deposition Rate Additive Manufacture of Nickel Superalloys and Metal Matrix Composites: University of Warwick, Warwick Manufacturing Group.” (2016).

[27] P. Mithilesh, D. Varun, Ajay Reddy Gopi Reddy, K. Devendranath Ramkumar, N. Arivazhaga, S. Narayanan. “Characterization of Microstructure and Mechanical Investigations on Dissimilar Weldments of Inconel 625 and AISI 304.” Procedia Engineering Vol. 75 No. 75 (2014): pp. 66–70. DOI 10.2355/isijinternational.54.900.

[28] T. DebRoy, H.L. Wei, J.S. Zuback, T. Mukherjee, J.W. Elmer, J.O. Milewski, A.M. Beese, A. Wilson-Heid, A. De, W. Zhang. "Additive manufacturing of metallic components – Process, structure and properties" Progress in Materials Science Vol. 92 (2018): pp. 112-224. DOI doi.org/10.1016/j.pmatsci.2017.10.001

[29] X. Wang, X. Gong, K. Chou. "Review on powder-bed laser additive manufacturing of Inconel 718 parts" Journal of Engineering Manufacture (2016) pp.1-14 DOI: 10.1177/0954405415619883

[30] R.D. Doherty, D.A. Hughes, F.J. Humphreys, J.J. Jonas, D. Juul Jensen, M.E. Kassner, W.E. King, T.R. McNelley, H.J. McQueen, A.D. Rollett, "Current issues in recrystallization: A review" Materials Science and Engineering A Vol. 238(2) (1997) pp. 219-274. DOI: 10.1016/S0921-5093(97)00424-3

[31] K.N. Amato, S.M. Gaytan, L.E. Murr, E. Martinez, P.W. Shindo, J. Hernandez, S. Collins, F. Medina. "Microstructures and mechanical behavior of Inconel 718 fabricated by selective laser melting" Acta Materialia Vol. (2012) pp. 2229-2239.

[32] S. Luo, W. Huang, H. Yang, J. Yang, Z. Wang, X. Zeng. "Microstructural evolution and corrosion behaviors of Inconel 718 alloy produced by selective laser melting following different heat treatments" Additive Manufacturing Vol. 30 (2019) pp. 100875 (1-13)

[33] C. Li, R. White, Y. Fang, M. Weaver, Y.B. Guo. "Microstructure evolution characteristics of Inconel 625 alloy from selective laser melting to heat treatment" Materials Science and Engineering A Vol, 705 (2017) pp.20-31.